Passing Current through Touching Molecules

Guillaume Schull,[1,*] Thomas Frederiksen,[2] Mads Brandbyge,[3] and Richard Berndt[1]

[1]*Institut für Experimentelle und Angewandte Physik, Christian-Albrechts-Universität zu Kiel, D-24098 Kiel, Germany*
[2]*Donostia International Physics Center (DIPC), E-20018 Donostia-San Sebastián, Spain*
[3]*DTU Nanotech, Technical University of Denmark, DK-2800 Kongens Lyngby, Denmark*

(Received 21 July 2009; published 11 November 2009)

The charge flow from a single C_{60} molecule to another one has been probed. The conformation and electronic states of both molecules on the contacting electrodes have been characterized using a cryogenic scanning tunneling microscope. While the contact conductance of a single molecule between two Cu electrodes can vary up to a factor of 3 depending on electrode geometry, the conductance of the C_{60}-C_{60} contact is consistently lower by 2 orders of magnitude. First-principles transport calculations reproduce the experimental results, allow a determination of the actual C_{60}-C_{60} distances, and identify the essential role of the intermolecular link in bi- and trimolecular chains.

DOI: 10.1103/PhysRevLett.103.206803 PACS numbers: 73.63.−b, 61.48.−c, 68.37.Ef

Intermolecular charge transport is central to numerous research fields. In biology electron hopping and tunneling processes between molecules play a vital role. Moreover, tunneling processes between molecular materials have opened new perspectives towards the realization of efficient molecular sensors and solar cells [1]. In a parallel direction the conductance properties of point contacts [2], single atoms [3], or single molecules [4] are intensely being investigated, and give a detailed view of charge transport through individual nanoscopic objects. Recently, experiments realized on 1D extended molecules [5], single conjugated polymers [6], and DNA wires [7] have been reported. A critical issue is now to understand and control the charge transfer from a single molecule to another one.

Here we probe the current passing through a chain of two C_{60} molecules suspended in a STM junction, where the orientation and electronic states of both molecules have been characterized before connecting them with atomic-scale precision. The experimental results are complemented by first-principles transport calculations which give access to the distance-dependent nature of the intermolecular electron transport and predict the evolution of the transport properties with molecular chain length.

The experiments were performed with a low-temperature STM operated at 5.2 K in ultrahigh vacuum. Au(111) and Cu(111) samples and etched W tips were prepared by Ar^+ bombardment and annealing. As a final preparation, W tips were indented into the sample surface to coat them with surface material. C_{60} molecules were deposited from a Ta crucible onto the sample at room temperature. The data shown correspond to a coverage of approximately 0.2 C_{60} monolayers. All images were recorded in a constant-current mode.

Increased image resolution with molecule-covered STM tips has repeatedly been reported [8]. However, no detailed information about the molecular orientation or their electronic properties was available. To realize controlled molecular contacts, these details are decisive. We used C_{60} molecules as their orientation can be determined from submolecularly resolved STM images [9,10]. Figure 1(a) shows a STM image, recorded with a metallic tip, of an array of C_{60} on a Au(111) surface. Two C_{60} orientations are observed, which are typical of a $(2\sqrt{3} \times 2\sqrt{3})R30°$ C_{60} superlattice [11].

To attach a C_{60} molecule to the tip, the metallic tip was placed over a target molecule and the sample voltage was varied from 2 to 0.01 V and back at a constant current $I =$ 100 nA. The success of this procedure can be verified from the removal of the molecule from the substrate (e.g., missing C_{60} in Fig. 1(b), black arrow). To further characterize C_{60} tips, structures composed of one (α) and two or three (β) Au adatoms had been deposited by slight contacts of the metallic STM tip with a clean surface area [Fig. 1(a), upper left] [12]. The image of Fig. 1(b) was obtained with a C_{60} functionalized tip over the same area. The Au clusters, which appear round and featureless with a metallic tip, exhibit a complex pattern which matches the highest occupied molecular orbital (HOMO) of C_{60} [9]. Obviously the Au adatoms work as tips for "reverse" imaging of C_{60} at

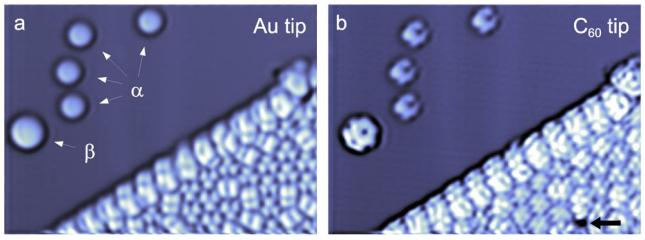

FIG. 1 (color online). STM images ($I = 10$ nA; $V = 2.5$ V; 14×11 nm^2) of Au(111) partially covered with C_{60} molecules (lower right) obtained with a (a) metal and (b) C_{60} tip over the same area. Gold adatoms (α) and a small gold cluster (β) of two or three adatoms are discernible.

the tip and provide direct access to the orientation of the molecule, e.g., in Fig. 1(b), a 6:6 bond of the C_{60} tip is facing the surface. While this technique has previously been used to determine the number of molecules adsorbed on a STM tip [13], the characterization of submolecular structures was not reported.

To monitor the density of states of C_{60} tips, Fig. 2 displays conductance spectra obtained with (a) a metallic tip on C_{60} and (b) a "reverse" spectrum recorded with a C_{60} tip on bare Au. The spectral peaks are characteristics of the molecular orbitals of C_{60} on Au(111) [11]. The spectra are almost perfect mirror images of each other reflecting that the electronic state of C_{60} at the tip is closely related to those of C_{60} on the surface. "Reverse" images and conductance maps of atomic sized clusters exhibit submolecular patterns [Figs. 2(c)–2(h)] which are typical of the lowest unoccupied molecular orbitals (LUMO + 1, $V \approx -2.5$ V and LUMO, $V \approx -1$ V) and HOMO ($V \approx 2$ V) [9,11]. Once a molecule is attached to the tip it is possible to change its orientation by passing current of up to ≈ 1 μA as demonstrated in Figs. 2(i)–2(l). The molecular patterns obtained correspond to different C_{60} orientations at the tip. While this sequence demonstrates control over the orientation of the tip molecule it also highlights an instability of these tips at high currents, which, therefore, were not suitable for the intended contact experiments. We repeated the previous experiments on C_{60} deposited on a Cu(111) substrate [Fig. 3(a)] where the binding of C_{60} is stronger [11]. Transfer of C_{60} from the Cu(111) to the Cu-covered tip remains feasible, although

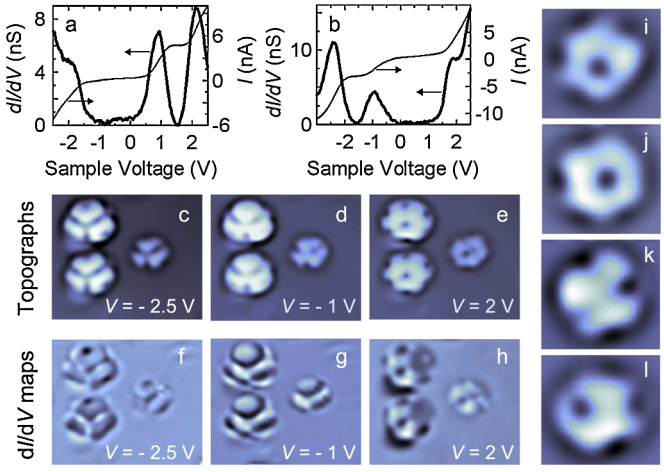

FIG. 2 (color online). Differential conductance (dI/dV) spectra acquired over (a) a C_{60} with a metal tip and (b) the bare metal with a C_{60} tip. (c)–(e) are reverse STM images ($I = 10$ nA; 5×4.2 nm^2) acquired over α and β type atomic clusters with a C_{60} tip at the voltages corresponding to peaks in the spectra of (b). (f)–(h) are dI/dV maps acquired simultaneously with the images. Reverse STM images (i)–(l) of a Au adatom with a C_{60} tip ($V = 2.5$ V; 1.5×1.4 nm^2). Between image acquisitions, the tip was moved to the surface so as to reach $I \approx 1$ μA, where reorientation of the C_{60} at the tip occurred.

the procedure is less reproducible than for Au(111) and μA currents are required. As in the Au case, the structural and electronic properties of the C_{60} tips have been characterized [Fig. 3(b)].

After characterization, metal and C_{60} tips were approached to C_{60} molecules and pristine Cu(111) areas and conductance-distance [$G(z)$] data were recorded [Fig. 3(c)]. No reorientation of the molecules occurred. Curve 1 was obtained with a sharp metallic tip approaching a C_{60} molecule. The right part of the trace corresponds to the tunneling range. Contact is indicated by an inflection of the trace, which defines a contact conductance of $0.3G_0$ (conductance quantum $G_0 = 2e^2/h$) in agreement with previous measurements on similar systems [4,14]. Curve 2 represents a measurement with a C_{60} tip approaching pristine Cu. Surprisingly, the contact conductance of $1.0G_0$ (G up to $\approx 1.5G_0$ were observed for different C_{60}

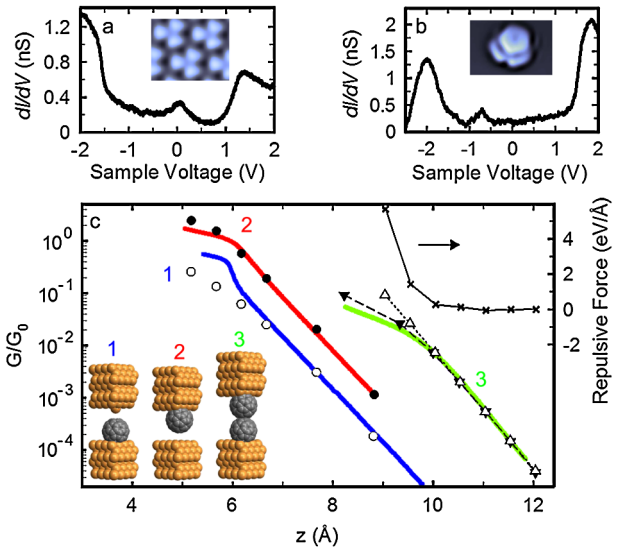

FIG. 3 (color online). (a),(b) dI/dV spectra acquired over (a) a C_{60} molecule on Cu(111) with a metal tip and (b) the bare metal with a C_{60} tip. Insets show (a) a STM image ($V = 2$ V; 2×1.6 nm^2) of a C_{60} array on Cu(111), where all molecules expose hexagons to vacuum, and (b) a reverse STM image ($V = -2$ V; 2.7×1.8 nm^2) of the C_{60} tip used for the contact experiment (a 5:6 bond is exposed to the surface). The inset to (c) displays sketches of the contact experiments performed by approaching (1) a sharp metallic tip to a C_{60} adsorbed on a hexagon on Cu(111), a 5:6 oriented C_{60} tip (2) to the bare Cu(111) surface and (3) to a C_{60} adsorbed on a hexagon. (c) Experimental (solid lines) and calculated (symbols) conductances versus distance. In cases (1) and (2), z is measured from the C_{60} center to the center of the outermost atom of the other electrode. In case (3), z is the C_{60} center to C_{60} center distance. This corresponds to an offset of ≈ 0.36 nm, i.e., half of the maximum atomic distance within the C_{60} cage. The calculated repulsive force (crosses) between two C_{60} molecules suggests an elastic deformation of the junction at small separations that maps real molecule-molecule distances (open triangles) with apparent distances (filled triangles). Sample voltages: (1) 100 mV; (2) -100 mV; (3) 200 mV.

orientations) is substantially higher than with C_{60} on the surface.

To understand the measured conductance traces first-principles transport simulations were carried out. We modeled the fullerene junctions by supercells with one or more C_{60} molecules bridging a 4×4 representation of a slab containing 13 Cu(111) layers. The electronic structure was determined with the SIESTA pseudopotential density functional theory (DFT) code [15] to calculate the transport properties for the TRANSIESTA setup [16]. For details, cf. Ref. [17]. Case 1 was modeled with a C_{60} adsorbed on a hexagon on the substrate side centered underneath a Cu adatom on the tip side, and case 2 with a C_{60} adsorbed on a 5:6 bond on the tip side facing a clean Cu(111) surface. For a transparent interpretation of the experiments we have considered the tip-molecule (sample-molecule) separation as the only variable in case 1 (case 2), and full geometry relaxations were not performed. Except for the structural rearrangements expected with a sharp metallic tip (case 1) [14], this approach reproduces and explains the observed traces. The calculated zero-bias conductances [Fig. 3(c)] enable a calibration of the absolute distances z (outermost Cu atom to C_{60}-center along the surface normal) between tip (sample) and molecule in case 1 (2) by aligning the tunneling part of the traces. Comparison of cases 1 and 2 shows that for a given distance z, depending on the geometry of the molecule-electrode interface, the conductance of a single C_{60} junction can vary by a factor of 3 (10) under contact (tunneling) conditions. The conductance of the C_{60}/Cu(111) junctions is dominated by the molecular LUMO resonances that lie closest to the Fermi energy E_F. The theoretical maximum is therefore $3G_0$ corresponding to three fully open conductance eigenchannels [16]. Indeed, a decomposition $T = \sum_i T_i$ of the total transmission $T = T(E_F)$ into eigenchannel contributions $\{T_i\}$ confirms that the three most transmitting channels carry about an order of magnitude more current than the fourth. For the sharp-tip contact (case 1 in Fig. 3) the transmissions in contact are of the order of $\{T_i\} \approx \{0.12, 0.08, 0.04, 0.004\}$; hence, the majority of an incoming electron wave is being reflected in this type of junction. Contrary, for the C_{60}-tip contact (case 2 in Fig. 3), three channels are much more open, theoretically in one case as much as $\{T_i\} \approx \{0.97, 0.87, 0.57, 0.02\}$.

To find out *where* the electrons are being scattered, Fig. 4(a) visualizes the most transmitting eigenchannel wave function for the different contacts [18]. Since the absolute square of the wave function corresponds to the density of the traversing electrons, the magnitude of the lobes gives an idea where the electron wave travels. In case 1 (sharp tip) the current is scattered at the single-atom contact to the molecule as indicated by the standing wave pattern at the tip side. In case 2 (C_{60} tip) the channel is almost perfectly open and the wave is propagating with essentially equal amplitude on either side of the molecule.

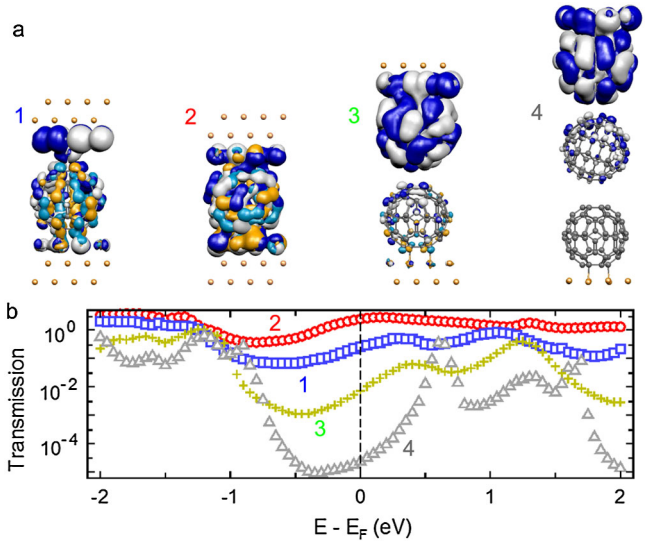

FIG. 4 (color online). (a) Visualizations of the most transmitting eigenchannel wave function (incoming from above) around E_F. Isosurfaces of the real and imaginary parts of the wave function (with sign). White and dark blue (black) corresponds to the real part and orange (light gray) and light blue (darker gray) to the imaginary part. (b) Calculated transmission of suspended chains of one, two, or three C_{60}. The molecular orientations are (1) adatom vs hexagon, (2) 5:6 bond vs flat surface, (3) hexagon vs 5:6 bond, and (4) hexagon vs 5:6 bond vs hexagon.

To disentangle the effects of different molecular orientation as well as of different atomic contacts on the conductance, we have carried out separate calculations with the hexagon orientation contacted with a flat tip. Specifically, between flat Cu(111) electrodes the 5:6 orientation was found to conduct slightly less than the hexagon orientation; e.g., at $z = 6.68$ Å the conductance is 19% lower for the 5:6 configuration. Moreover, experimental data from various C_{60} orientations [19] show that $0.3G_0$ (case 1) is already an upper limit of the conductance of C_{60} on a Cu surface contacted with a sharp STM tip. We therefore conclude that the higher conductance of $1.0G_0$ (case 2) is due to the multiple-atomic contact which ensures a better connection between the molecule and the electrode. This characterization of the metal-molecule contact could be valuable for fullerene-based anchoring strategies for molecular electronics [20].

Finally, the C_{60} tip of curve 2 in Fig. 3(c) was also approached to a C_{60} molecule on the substrate. Yazdani *et al.* used a similar method to measure the conductance of diatomic xenon chain [21]. Employing the molecular orientations determined in the experiment, this case was modeled with a C_{60} adsorbed on a hexagon on the substrate side under a C_{60} adsorbed on a 5:6 bond on the tip side. Note that the displacement axis now shows the C_{60} to C_{60} center distance. The observed conductance trace [curve 3 in Fig. 3(c)] varies smoothly from tunneling to contact at a molecular separation of $\approx$1 nm. The contact conductance

of $\approx 0.01 G_0$ is an order of magnitude smaller than expected for a C_{60} dimer [22]. In contrast to the experimental observation of a plateau, our model predicts an exponential dependence of the conductance on the C_{60}-C_{60} separation [open triangles in Fig. 3(c)] and no significant influence of the C_{60}-surface distance (see Ref. [17]). This difference is due to an intermolecular repulsion at small distances that deforms the contact. Therefore, beyond the point of contact, the experimental data reflect *apparent* molecular separations, the actual distances being somewhat larger. To take into account the elastic deformation of the junction, repulsive forces were estimated from our DFT calculations [crosses in Fig. 3(c)]. By renormalizing the theoretical z coordinates according to the compliance of two soft molecule-surface segments (effective elastic constant 7 eV/Å) [17], we obtain agreement with the experimental trace [filled triangles in Fig. 3(c)]. While it is possible to further improve this agreement by considering the elasticity of the other parts of the system [17], the essential feature of the experiment is already captured by inclusion of just the softest segment. Interestingly, the onset of elastic deformation coincides with the intermolecular distance of 1.004 nm in C_{60} crystals, which is controlled by van der Waals bonding and electrostatic repulsion [23].

The picture emerging for chains of two C_{60} molecules is that the transport processes are mainly sensitive to the molecule-molecule interface. It is further supported by Fig. 4(a), part 3, which shows isosurfaces of the dominant eigenchannel with little weight on the lower molecule. This is due to a reduced wave function amplitude beyond the C_{60}-C_{60} interface, which thus acts as conductance bottleneck. Within the chain the intermolecular distance is limited by electrostatic repulsion. In this way the experiment is probing how current passes through two *touching* molecules, the properties and the nature of both being controlled and tunable.

Using the C_{60}-C_{60} contact distance determined above, the transport through a three-C_{60} chain was calculated. In this case the dominant eigenchannel Fig. 4(a), part 4, is strongly attenuated along the chain as revealed by the absence of lobes on the lower molecule. The transmission functions of the molecular chains Fig. 4(b) reveal the opening of a ~ 1.5 eV gap around E_F, and hence predict a rapid evolution towards an insulating infinite C_{60} chain.

In summary, the contact conductance for single C_{60} junctions can vary up to a factor of 3 depending on the molecule-metal interfaces, thus corroborating the notion of good and bad contacts. The current passing from one molecule to another one, however, is determined by the molecule-molecule interface. Our experimental approach can be extended to a range of molecules to address the influence of the molecule-molecule interactions on intermolecular charge transport. Moreover, through detection of photons emitted in a STM junction [24], a suitable fluorescent molecule attached to the STM tip might prove useful as optically active probe [25].

Financial support via SFB 677, Innovationsfonds S-H, and FNU 272-07-0114 is gratefully acknowledged.

*Institut de Physique et de Chimie de Strasbourg, Université Louis Pasteur, CNRS UMR 7504, 67034 Strasbourg, France.

[1] M. E. El-Khouly *et al.*, J. Photochem. Photobiol. C **5**, 79 (2004); R. H. Goldsmith *et al.*, Proc. Natl. Acad. Sci. U.S.A. **102**, 3540 (2005).
[2] A. G. M. Jansen *et al.*, J. Phys. C **13**, 6073 (1980).
[3] C. J. Muller *et al.*, Phys. Rev. Lett. **69**, 140 (1992).
[4] C. Joachim *et al.*, Phys. Rev. Lett. **74**, 2102 (1995).
[5] S. Ho Choi *et al.*, Science **320**, 1482 (2008).
[6] L. Lafferentz *et al.*, Science **323**, 1193 (2009).
[7] H. Cohen *et al.*, Proc. Natl. Acad. Sci. U.S.A. **102**, 11589 (2005).
[8] Q.-M. Xu *et al.*, J. Phys. Chem. B **105**, 10465 (2001); T. Nishino *et al.*, Proc. Natl. Acad. Sci. U.S.A. **102**, 5659 (2005); J. Repp *et al.*, Phys. Rev. Lett. **94**, 026803 (2005).
[9] X. Lu *et al.*, Phys. Rev. Lett. **90**, 096802 (2003).
[10] G. Schull and R. Berndt, Phys. Rev. Lett. **99**, 226105 (2007).
[11] G. Schull *et al.*, New J. Phys. **10**, 065012 (2008).
[12] L. Limot *et al.*, Phys. Rev. Lett. **94**, 126102 (2005).
[13] K. F. Kelly *et al.*, J. Vac. Sci. Technol. B **14**, 593 (1996).
[14] N. Néel *et al.*, Phys. Rev. Lett. **98**, 065502 (2007).
[15] J. M. Soler *et al.*, J. Phys. Condens. Matter **14**, 2745 (2002).
[16] M. Brandbyge *et al.*, Phys. Rev. B **65**, 165401 (2002).
[17] See EPAPS Document No. E-PRLTAO-103-005947 for supplementary material. For more information on EPAPS, see http://www.aip.org/pubservs/epaps.html.
[18] M. Paulsson and M. Brandbyge, Phys. Rev. B **76**, 115117 (2007).
[19] N. Néel *et al.*, Nano Lett. **8**, 1291 (2008).
[20] C. A. Martin *et al.*, J. Am. Chem. Soc. **130**, 13198 (2008).
[21] A. Yazdani *et al.*, Science **272**, 1921 (1996).
[22] T. Ono and K. Hirose, Phys. Rev. Lett. **98**, 026804 (2007).
[23] W. I. F. David *et al.*, Europhys. Lett. **18**, 219 (1992).
[24] G. Schull *et al.*, Phys. Rev. Lett. **101**, 136801 (2008).
[25] J. Michaelis *et al.*, Nature (London) **405**, 325 (2000).

Supplementary material

Theoretical details. The electronic structure for the supercells shown in the inset of Fig. 3c was calculated with the SIESTA[1] pseudopotential density functional theory (DFT) method and the generalized gradient approximation[2] for exchange-correlation (XC). A standard single-zeta plus polarization basis was employed for Cu (0.15 eV energy shift, $r_c \leq 6.9$ a.u.) and a long-ranged, double-zeta plus polarization basis for C (0.02 eV energy shift, $r_c \leq 5.5$ a.u.). Real-space grid integrations were carried out using a 200 Ry energy cutoff. The 3D Brillouin zone was sampled with a $2 \times 2 \times 1$ Monkhorst-Pack **k**-mesh. The lattice constant for the Cu crystal was set to 3.70 Å. An initial structure consisting of a C_{60} molecule adsorbed with a hexagon on an hcp hollow-site on a slab containing 7 Cu(111) layers, was fully relaxed until all forces on the molecule, the adatom placed on the reverse side of the slab, and the surface layer, were smaller than 0.02 eV/Å. Based on this configuration and the molecular orientations derived from the experiment we constructed the supercells shown in Fig. 3c for several different electrode separations. These supercells were not relaxed; forces up to a few eV/Å were thus tolerated.

The electronic structure from SIESTA was used to calculate the transport properties for the TranSIESTA[3] setup. The zero-bias conductance $G = G_0 T(E_F)$ was derived from the transmission function $T(E)$ calculated by Green's function techniques involving the Kohn-Sham Hamiltonian in the scattering region and self-energies representing atomistic, semi-infinite electrodes obtained from separate calculations for bulk Cu(111). The transmission was sampled over a 6×6 $\mathbf{k}_{||}$-mesh for the 2D Brillouin zone. To check the parameters described above, we carried out calculations for a representative structure with increased number of **k**-points for both the electronic structure part as well as for the transmission. The variations in the zero-bias conductance were $\leq 6\%$. The eigenchannel visualizations, shown in Fig. 4a, were calculated at the Fermi energy E_F for the Γ-point according to the scheme presented in Ref. 4. As seen in Fig. 4b the transmission functions vary smoothly over the energy scale of the experimentally applied voltages. This justifies the comparison with the calculated zero-bias conductances.

Elastic response of the C_{60}–C_{60} junction.. The theoretical data in Fig. 3c show that the conductance of the C_{60}–C_{60} junction depends exponentially on the intermolecular separation, approximately as $G(z) \propto e^{-2.6\text{Å}^{-1} z}$. To prove that the conductance does not depend significantly on the molecule–substrate distance, we varied the electrode separation by ±0.50 Å for a fixed (realistic) C_{60}–C_{60} distance of $z = 9.54$ Å, only to find the conductance changed by less than 9%. In comparison, varying the intermolecular separation by the same amount, the conductance changes by a factor 3.7. The experimental observation of a plateau after contact formation is therefore related to an elastic deformation of the junction, driven by a strong intermolecular repulsion between the two molecules.

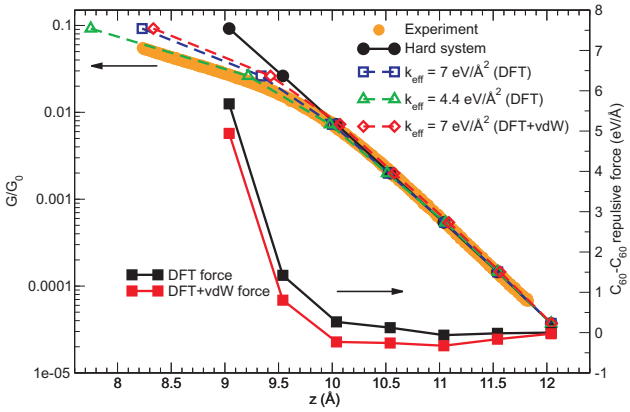

FIG. S1: Conductance traces and intermolecular forces for the C_{60}–C_{60} junction with different estimates of the elasticity of the system and the C_{60}–C_{60} repulsion (with and without van der Waals contributions).

To estimate the C_{60}–C_{60} repulsion in our structures we determined the average force $(F_z^{(2)} - F_z^{(1)})/2$, where $F_z^{(i)}$ is the z-component of the sum of atomic forces on molecule i from our DFT calculations. Taking the setup with the largest intermolecular separation as a point of reference, the evolution of intermolecular repulsion within DFT is represented in Figs. 3c and S1. For an elastic system, characterized by the effective elastic constant k_{eff} arising from a series of springs ($1/k_{\text{eff}} = \sum_i 1/k_i$), the STM piezo distances can thus be related to intermolecular distances via $z_{\text{piezo}} = z_{\text{inter}} - F/k_{\text{eff}}$. One example of such coordinate renormalization is shown in Fig. 3c where only the two soft molecule–surface segments were included ($k_{\text{eff}} = k_{\text{m-s}}/2$). One can refine this description by including C_{60} compressions ($k_{\text{mol}} \sim 108$ eV/Å^2 for each C_{60}) and the compliance of the metal surfaces ($k_{\text{surf}} \sim 30$ eV/Å^2 for each electrode), which leads to $k_{\text{eff}} = 4.4$ eV/Å^2 and an a very good agreement with the experimental data, cf. triangles in Fig. S1.

While short-range interactions are generally well-described in DFT with standard local approximations for XC, the long-range van der Waals (vdW) interactions are not easily incorporated in DFT because of its nonlocality. Therefore, to get an estimate of the vdW contributions to the forces in the C_{60}–C_{60} contact (case 3 in Fig. 3), we applied an empirical correction following Ref. 5. In this scheme the interaction energy between each pair of atoms (i, j), separated by the distance R, is corrected by an additional attractive energy the form $U_{ij}^{\text{vdW}} = -f_D^{ij}(R) C_6^{ij}/R^6$, where $f_D^{ij}(R) = 1 - \exp[-0.00075 R^8/(r_i + r_j)^8]$ is a damp-

ing function that removes contributions for small separations. The parameter r_i is a characteristic covalent radius of atom i. We used $r_{\mathrm{C}} = 0.7245$ Å (corresponding to the average bond length in our description of C_{60}) and $r_{\mathrm{Cu}} = 1.308$ Å (derived from the Cu lattice constant). For the C_6 coefficient we used the London formula $C_6^{ij} = \frac{3}{2}\alpha_i\alpha_j I_i I_j/(I_i + I_j)$ with experimental values[6] for the polarizability α_i and the ionization potential I_i of atom i. The strategy outlined above enabled us to reproduce the 3D fcc crystal of C_{60} with a lattice constant of 10.02 Å and a bulk modulus only about 12% lower than the experimental value. Applying the vdW correction to the C_{60}–C_{60} contact the forces shown in Fig. S1 are obtained. Since the intermolecular repulsion is only slightly reduced by the attractive vdW forces, the coordinate renormalization of the conductance trace is mostly sensitive to the elastic constant k_{eff} and not to the force estimate. Furthermore, since it is generally argued that the London form shows a tendency to overestimate the vdW interaction [see Ref. 5 and references herein], we conclude that vdW contributions play a minor role for understanding the experimental conductance trace.

[1] J. M. Soler, E. Artacho, J. D. Gale, A. Garcia, J. Junquera, P. Ordejon, and D. Sanchez-Portal, J. Phys.: Condens. Matter **14**, 2745 (2002).

[2] J. P. Perdew, K. Burke, and M. Ernzerhof, Phys. Rev. Lett. **77**, 3865 (1996).

[3] M. Brandbyge, J. L. Mozos, P. Ordejon, J. Taylor, and K. Stokbro, Phys. Rev. B **65**, 165401 (2002).

[4] M. Paulsson and M. Brandbyge, Phys. Rev. B **76**, 115117 (2007).

[5] F. Ortmann, F. Bechstedt, and W. G. Schmidt, Phys. Rev. B **73**, 205101 (2006).

[6] *CRC Handbook of Chemistry and Physics, 80th edition*, edited by D. R. Lide (CRC, ISBN: 0-8493-0480-6, 1999).